

See discussions, stats, and author profiles for this publication at: <https://www.researchgate.net/publication/311362295>

# ChaC2: An Enzyme for Slow Turnover of Cytosolic Glutathione

Article in *Journal of Biological Chemistry* · December 2016

DOI: 10.1074/jbc.M116.727479

CITATIONS

34

READS

452

7 authors, including:



**Amandeep Kaur Deol**

Indian Institute of Science Education & Research Mohali

5 PUBLICATIONS 253 CITATIONS

[SEE PROFILE](#)



**Ruchi Gautam**

Institute of Microbial Technology

4 PUBLICATIONS 55 CITATIONS

[SEE PROFILE](#)



**Avinash Chandel**

University of California, Santa Barbara

10 PUBLICATIONS 84 CITATIONS

[SEE PROFILE](#)



**Anand Bachhawat**

Indian Institute of Science Education & Research Mohali

92 PUBLICATIONS 1,555 CITATIONS

[SEE PROFILE](#)

Some of the authors of this publication are also working on these related projects:



CSmetaPred: A consensus method for prediction of catalytic residues [View project](#)



I am currently working on regulation of glycolytic enzymes under stress conditions [View project](#)

## ChaC2: An Enzyme for Slow Turnover of Cytosolic Glutathione

Amandeep Kaur<sup>1+</sup>, Ruchi Gautam<sup>2+</sup>, Ritika Srivastava<sup>2+</sup>, Avinash Chandel<sup>1</sup>, Akhilesh Kumar<sup>1,3</sup>, Subramanian Karthikeyan<sup>2\*</sup> and Anand Kumar Bachhawat<sup>1\*</sup>

<sup>1</sup>From the Department of Biological Sciences, Indian Institute of Science Education and Research, Mohali, S.A.S. Nagar, Punjab 140306, India

<sup>2</sup>CSIR-Institute of Microbial Technology, Council of Scientific and Industrial Research (CSIR), Sector 39A, Chandigarh 160036, India

<sup>3</sup>Present address: University of Miami Miller School of Medicine, Florida

<sup>+</sup>Equal contribution

Running title: Structure and function of ChaC2

\*Corresponding authors: Anand Kumar Bachhawat, [anand@iisermohali.ac.in](mailto:anand@iisermohali.ac.in), Tel: +91-172-2240119, Fax: +91-172-2240266. Subramanian Karthikeyan, [skarthik@imtech.res.in](mailto:skarthik@imtech.res.in), Tel: +91-172-6665193, Fax: +91-172-2690585.

**Keywords:** ChaC1,  $\gamma$ -Glutamylcyclotransferase fold; ChaC; ChaC2; GCG1; glutathione degradation; crystal structure.

### ABSTRACT

Glutathione degradation plays an important role in glutathione and redox homeostasis and thus it is imperative to understand the enzymes and the mechanisms involved in glutathione degradation in detail. We describe here ChaC2, a member of the ChaC family of  $\gamma$ -glutamylcyclotransferases, as an enzyme that degrades glutathione in the cytosol of mammalian cells. ChaC2 is distinct from the previously described ChaC1, to which ChaC2 shows about 50% sequence identity. Human and mouse ChaC2 proteins, purified *in vitro*, show 10-20 fold lower catalytic efficiency than ChaC1, although they showed comparable  $K_m$  values ( $K_m$  of  $3.7 \pm 0.4$  mM and  $k_{cat}$  of  $15.9 \pm 1.0$  min<sup>-1</sup> towards glutathione for human ChaC2;  $K_m$  of  $2.2 \pm 0.4$  mM and  $k_{cat}$  of  $225.2 \pm 15$  min<sup>-1</sup> towards glutathione for human ChaC1). The ChaC1 and ChaC2 proteins also shared the same specificity for reduced glutathione, with no activity against either  $\gamma$ -glutamyl amino acids or oxidized glutathione. The ChaC2 proteins were found to be expressed constitutively in cells, unlike the tightly regulated ChaC1. Moreover, lower eukaryotes have a single member of the ChaC family that appears to be orthologous to ChaC2. In addition, we determined the crystal

structure of yeast ChaC2 homologue, GCG1 at 1.34 Å resolution which represents the first structure of the ChaC family of proteins. The catalytic site is defined by a fortuitous benzoic acid molecule bound to the crystal structure. The mechanism for binding and catalytic activity of this new enzyme of glutathione degradation, which is involved in continuous, but basal turnover of cytosolic glutathione, is proposed.

Glutathione is an essential metabolite in almost all eukaryotic cells; the only exceptions are the amitochondrial protozoans (1). In addition to the essential role in mitochondrial iron-sulphur biogenesis (2), glutathione plays many other roles, that include its role as the principal redox buffer (2,3), in sulphur storage and transport, xenobiotic, metal and ROS detoxification (4,5), and its ability to regulate protein function through glutathionylation (6). Glutathione is essential in eukaryotes and knocking out glutathione biosynthesis is embryonically lethal in mammals (7). Furthermore, glutathione depletion is a hallmark of apoptosis (8) and low glutathione levels have been strongly correlated with several disease states (9). However, high levels of glutathione are also deleterious to the cell (10-13). Thus, it is important for the cell to

ensure that the levels of glutathione are tightly regulated. Glutathione degradation and turnover is an important factor in glutathione homeostasis (14). However, for several decades, only a single enzyme,  $\gamma$ -glutamyltranspeptidase, was shown to be responsible for glutathione degradation, but its effects were on non-cytosolic pools of glutathione (15). Recent studies have led to the discovery of two new enzymes for cytosolic glutathione degradation. The first is the Dug enzyme consisting of the (Dug2p-Dug3p)<sub>2</sub> enzyme complex that can specifically breakdown glutathione to Cys-Gly and glutamate (16,17). This pathway is exclusively present in yeast and fungi. The second pathway involves the ChaC1 enzyme, a member of the ChaC family of  $\gamma$ -glutamylcyclotransferases that can specifically degrade glutathione to 5-oxoproline and Cys-Gly (10) and is induced under conditions of ER stress in the cell (10,18). Members of the ChaC family have been found in organisms ranging from the unicellular bacteria and yeast to the higher multicellular eukaryotes such as *Drosophila melanogaster*, mouse and humans. In *E. coli* and yeast, a single homologue of ChaC has been found to exist. However, in the higher multicellular eukaryotes, two ChaC homologues are present, ChaC1 and ChaC2. While the mouse, and human ChaC1 function as glutathione degrading enzymes (10,19), the function of the mammalian ChaC2 proteins have not been explored.

In this manuscript, we have investigated the function of ChaC2, and determined that it functions in glutathione degradation similar to ChaC1 proteins. However, the ChaC2 proteins are characterized by a far lower catalytic efficiency than ChaC1, and unlike ChaC1, are constitutively expressed. Furthermore, the single ChaC homologue present in lower eukaryotes and prokaryotes appears to be functionally equivalent to the ChaC2 rather than the ChaC1. In addition, we have solved the crystal structure of the ChaC2 homologue in yeast. This is the first crystal structure to be determined for any member of the ChaC family of proteins and thus provides insights into the mechanism of action of ChaC proteins.

## RESULTS

*Sequence analysis and phylogeny suggests ChaC1 and ChaC2 represent two distinct members of the ChaC family:-* The amino acid sequence of mouse ChaC1 and mouse ChaC2 display about 50% identity between them. Similarly human ChaC1 shows 50% identity to the human ChaC2. In contrast when mouse ChaC1 was compared with human ChaC1 there was an 88% sequence identity, and mouse ChaC2 compared with human ChaC2 reveals an approximately 94% identity between the proteins (data not shown). This suggested that the ChaC1 and ChaC2 proteins might represent two distinct members of the ChaC family. To investigate this further we built a phylogenetic tree with members of the ChaC family proteins from different organisms. The phylogenetic tree strongly suggests that the ChaC family consists of two different branches represented by the ChaC1 and ChaC2 proteins (Figure 1). Interestingly, we observed that, the higher eukaryotes had both ChaC1 and ChaC2 members, while some of the lower eukaryotes such as *Caenorhabditis elegans*, yeast such as *Saccharomyces cerevisiae*, fungi, and unicellular protozoans such as *Tetrahymena thermophila* and bacteria such as *E. coli* had a single ChaC.

*The human ChaC2 functions specifically in glutathione degradation:-* To make a preliminary evaluation into the function of ChaC2, we cloned the human ChaC2 and evaluated its function by simple growth-based functional assays that evaluate glutathione degradation in yeast. ChaC2 expressed downstream of the yeast constitutive TEF promoter in the centromeric p416TEF vector was transformed into the yeast *S. cerevisiae* ABC 1723 and the transformants were evaluated for their growth on either the sulphur containing dipeptides  $\gamma$ -glutamylmethionine and  $\gamma$ -glutamylcystine or the tripeptide,  $\gamma$ -glutamylcysteinyl-glycine (glutathione) as sulphur source. This strain is an organic sulphur auxotroph due to the *met15 $\Delta$*  (leads to a defect in inorganic sulphur assimilation pathway) and cannot utilize glutathione due to the presence of the deletions *ecm38 $\Delta$*  ( $\gamma$ -glutamyltranspeptidase gene) and *dug3 $\Delta$*  (component of the DUG enzyme). The strain thus allows to check the glutathione degrading capability of ChaC2

proteins. We observed that the human ChaC2 expressed in yeast could allow growth only on glutathione, but could not grow on either of the two  $\gamma$ -glutamyl-dipeptides,  $\gamma$ -Glu-Met or  $\gamma$ -Glu-Cys. Human ChaC1 was also evaluated on these different substrates and was found to act with a similar specificity on glutathione as had been observed with the mouse ChaC1 (Figure 2A). To examine the relative efficiencies with which they acted on glutathione within the cell, the human ChaC2 and human ChaC1 bearing constructs were expressed in a yeast strain with a defect in glutathione biosynthesis to see how they retarded growth on low glutathione supplementation. Both the proteins led to retarded growth of these strains, although human ChaC1 was more efficient than ChaC2 in depleting glutathione levels *in vivo* as seen from the growth patterns (Figure 2B). To further evaluate the effects of human ChaC2 and ChaC1 *in vivo*, we estimated the reactive oxygen species (ROS) levels in cells transformed with either human ChaC2 or ChaC1. The over-expression of human ChaC1 led to 80% increase in ROS levels while with human ChaC2 it was only a 28% increase in ROS levels (Figure 2C). These results indicate that along with the increased depletion of glutathione that was occurring with ChaC1 overexpression, a corresponding increase in ROS was also seen, while in the less efficient ChaC2, a lower depletion of glutathione, and a consequent lower increase in ROS was observed. To confirm that the increased ROS was a consequence of lower glutathione levels, we also directly estimated glutathione levels in cells that had ongoing glutathione biosynthesis. ChaC1 overexpressing cells showed a significantly lower glutathione level as compared to controls, while ChaC2 expressing cells showed only a small decrease in glutathione levels (Figure 2D).

*The purified human and mouse ChaC2 proteins degrade glutathione at lower efficiency than their ChaC1 homologues in vitro:-* To evaluate the glutathione degradation capability of the ChaC2 proteins more rigorously, the human and mouse ChaC2 proteins were expressed in *E. coli* and purified as described in materials and methods. The purified proteins on SDS- PAGE displayed a size of 22 kDa and 21 kDa

respectively for the human and mouse proteins (data not shown), close to their predicted molecular size. In gel filtration studies, the ChaC2 showed a single monomeric peak (data not shown).

Enzyme assays to evaluate the efficiency of human ChaC2 on different  $\gamma$ -glutamyl compounds (compared with ChaC1), revealed that in *in vitro* also human ChaC2 displayed catalytic activity against glutathione but did not show any activity against either oxidised glutathione or  $\gamma$ -Glu-Cys (data not shown). The kinetics of the purified proteins were determined using the Dug1p-coupled assay. Human ChaC2 displayed Michaelis-Menten kinetics and showed a  $K_m$  of  $3.7 \pm 0.4$  mM and  $k_{cat}$  of  $15.9 \pm 1.0$  min<sup>-1</sup> towards glutathione (Figure 3A) while mouse ChaC2 similarly displayed Michaelis-Menten kinetics with a  $K_m$  of  $3 \pm 0.40$  mM and  $k_{cat}$  of  $7.6 \pm 0.5$  min<sup>-1</sup> towards glutathione (data not shown). Thus, the kinetic parameters of human and mouse ChaC2 were comparable and their  $K_m$  values appeared to be physiologically relevant considering glutathione is found at millimolar levels in the cell.

In comparison, the human ChaC1 showed a  $K_m$  of  $2.2 \pm 0.4$  mM and  $k_{cat}$  of  $225.2 \pm 15$  min<sup>-1</sup> towards glutathione (Figure 3B). As reported earlier, the mouse ChaC1 had a  $K_m$  of  $3.13 \pm 0.40$  mM (10) and  $k_{cat}$  of  $391 \pm 3.1$  min<sup>-1</sup>. Thus, while the  $K_m$  of both human ChaC2 and human ChaC1 were comparable and within the physiological range of glutathione concentrations in the cell, the  $k_{cat}$  of ChaC2 protein showed 10-20 fold lower catalytic efficiency than the human ChaC1 protein.

*Human ChaC2 is a cytosolic, constitutively expressed protein:-* To experimentally determine the localization of human ChaC2, anti-human ChaC2 antibodies were used to immunostain natively expressed ChaC2 in HEK cells. The results indicated that ChaC2 is localized in the cytosol (Figure 4).

To examine if the human ChaC2 expression was induced during ER stress similar to what had been observed with the mouse and human ChaC1 proteins, we subjected HEK cells to the

ER stress inducing agent tunicamycin. ChaC1 and ChaC2 mRNA levels were measured using real time qPCR and protein levels were measured using western blot analysis (Figure 5A, B). We observed that ER stress induces the expression of human ChaC1 significantly, as reported earlier, but no significant changes were observed in the case of human ChaC2.

Glutathione degradation also serves as source of sulphur for the cells. Hence, we investigated the effect of sulphur starvation on human ChaC1 and ChaC2 expression by real-time PCR analysis. As illustrated in Figure 5C we found that sulphur starvation upto 18hrs significantly increases ChaC1 transcription by about 10 fold but on further extension beyond 18 hrs the levels started decreasing which may be due to loss of cell viability. In comparison, in case of human ChaC2 there was no significant change in the levels. We also evaluated the expression levels at the protein level by western blot analysis where human ChaC1 levels increases significantly at 18 to 24 hrs of exposure but only a small increase in the levels of human ChaC2 was observed (Figure 5D).

In human breast and ovarian cancer cells human ChaC1 has been shown to be upregulated. We therefore examined whether human ChaC2 was found at higher levels in cancer cells. We carried out a comparison of human ChaC1 and ChaC2 RNA levels in HEK (non-tumourigenic) cells and various tumourigenic cell lines of different tissues origin. Higher levels of ChaC1 transcripts were present in all the tumourigenic cell lines as compare to HEK cells, even without the need for induction. In comparison to this, levels of human ChaC2 transcripts in tumourigenic cell lines were comparable to, or slightly less than the levels seen in HEK cells (Figure 6).

*E. coli* ChaC and yeast GCG1 also function as ChaC2-like proteins:- During the sequence and phylogenetic analysis it was evident that many of the unicellular eukaryotes and prokaryotes had a single homologue of the ChaC family. Moreover, sequence comparisons with the *S. cerevisiae* GCG1 protein (ORF YER163c; Yeast ChaC homologue) indicated that it had greater

similarity to the ChaC2 proteins. This was also reflected in the kinetic analysis. We had previously investigated the kinetics of the yeast GCG1 along with the mouse ChaC1 (10). The yeast GCG1 has been shown to be cytosolic (20). The  $K_m$  of GCG1 was found to be  $1.5 \pm 0.20$  mM (10) while the  $k_{cat}$  had a value of  $50.8 \text{ min}^{-1}$ . The  $k_{cat}$  was 9 fold lower than the  $k_{cat}$  of mouse ChaC1. The significance of this difference in  $k_{cat}$  was not recognized at that point since the ChaC1 and ChaC2 had not been defined as two distinct members of ChaC family earlier. In the case of few other organisms, such as *T. thermophila* and *E. coli* which also had a single homologue, it was not immediately clear from sequence similarities if the protein was a member of the ChaC1 or ChaC2 families. We decided to evaluate one of these proteins, the *E. coli* ChaC for its kinetic parameters. *E. coli* ChaC was earlier shown to specifically degrade glutathione (10), but its kinetic parameters were never evaluated. The purified *E. coli* ChaC protein was used to determine the kinetic parameters. The protein displayed Michaelis-Menten kinetics and the  $K_m$  and  $k_{cat}$  towards glutathione was found to be  $3.1 \pm 0.91$  mM and  $13 \pm 0.27 \text{ min}^{-1}$  respectively (Data not shown). The  $K_m$  being within the physiological range of glutathione suggested that the activity was physiologically relevant, while the  $k_{cat}$  indicates a lower catalytic efficiency than mouse and human ChaC1 but comparable efficiency to the mouse and human ChaC2. This suggested that the *E. coli* ChaC was functionally orthologous to the ChaC2 protein family.

*Crystallographic studies and quality of the yeast ChaC2 homolog (GCG1) model:-* To gain mechanistic insights we initiated the crystal structure determination of ChaC2 protein. The attempt to crystallize the human ChaC2 was unsuccessful. However, the crystallization of yeast GCG1 a homologue of human ChaC2 was successful and we were able to collect X-ray diffraction data upto  $2.2 \text{ \AA}$  from an in-house X-ray source. Despite many attempts we could not solve the structure by molecular replacement using the close homologs that were available in the Protein Data Bank (PDB) as templates. Therefore, we decided to determine the structure by anomalous dispersion method by incorporating selenomethionine residues in the

GCG1 protein. Since, the native GCG1 protein contained only three methionine residues, including the initial N-terminal methionine, we mutated additional four residues to methionine (S42M, L77M, A141M and V176M) to increase the chance of solving the structure by single or multiple anomalous dispersion (SAD or MAD) methods. The native GCG1 protein was overexpressed, purified and crystallized in P1 space group with unit cell parameters  $a=41.78$  Å,  $b=62.02$  Å,  $c=61.70$  Å and  $\alpha=113.71^\circ$ ,  $\beta=89.89^\circ$ ,  $\gamma=101.80^\circ$ . The calculation of Matthew's coefficient (21) and solvent content suggested two molecules in the asymmetric unit, with the values corresponding to  $2.7$  Å<sup>3</sup> Da<sup>-1</sup> and 55% respectively. Similarly, the semet-GCG1-mutant overexpressed in the presence of selenomethionine was purified and crystallized in P4<sub>2</sub>2<sub>1</sub>2 space group with unit cell parameters of  $a=b=110.55$  Å and  $c=42.59$  Å. Assuming one molecule per asymmetric unit, the calculated Matthew's coefficient was  $2.5$  Å<sup>3</sup> Da<sup>-1</sup> with 51% solvent content.

Initially, the crystal structure of semet-GCG1-mutant was solved by the single anomalous dispersion (SAD) method with one molecule in the asymmetric unit and the model was further refined using PHENIX suite of programs with final  $R_{\text{work}}$  and  $R_{\text{free}}$  (22) of 0.17 and 0.21 respectively. The model of semet-GCG1-mutant consists of 229 residues (out of 232), 142 water molecules and one succinic acid molecule. The crystal structure of native GCG1 was solved by molecular replacement method using the structure of semet-GCG1-mutant as template. The crystal structure of GCG1 showed two molecules in the asymmetric unit. The GCG1 model was further refined using PHENIX suite of programs with  $R_{\text{work}}$  and  $R_{\text{free}}$  converged to 0.16 and 0.19 respectively. The final GCG1 model consists of 445 residues (out of 464), 441 solvent molecules, two benzoic acid molecules and two phosphate ions. The initial N-terminal five residues and the residues from 210 to 214 were not included in the model due to lack of electron density. The calculated buried area ( $434$  Å<sup>2</sup>) at the interface using PISA (23) server indicated that the two molecules in the asymmetric unit does not form any stable oligomer which was consistent with our gel-

filtration studies and thus GCG1 exists as monomer in solution. The final refinement statistics for native and semet-GCG1-mutant structures are shown in Table 2.

*Overall three dimensional structure of GCG1:-* The crystal structure of GCG1 revealed that it belonged to the  $\gamma$ -glutamylcyclotransferase-like fold despite its low sequence similarity with other members of this family. The overall topology of GCG1 is shown in Figure 7 and mainly consists of seven antiparallel  $\beta$ -strands and six  $\alpha$ -helices. Earlier, the  $\gamma$ -glutamylcyclotransferase fold was defined with the features consists of a  $\beta$ -barrel topology with two strands "crossing over", a highly conserved helix, a binding cavity formed at one side of the  $\beta$ -barrel, a loop following strand  $\beta$ 1 containing a conserved (V/A)YG(S/T) motif, a conserved tyrosine in strand  $\beta$ 4, and an aromatic residue in strand  $\beta$ 5 (24). Essentially, all these features were present in GCG1 model with the  $\beta$ -barrel topology formed by the strands ( $\beta$ 1– $\beta$ 2– $\beta$ 5– $\beta$ 6– $\beta$ 7) with crossing over strands  $\beta$ 6 and  $\beta$ 7, the highly conserved helix  $\alpha$ -2, the loop following strand  $\beta$ 1 contains 12-GYGS-15motif, a conserved tyrosine (Y119) in  $\beta$ 6 strand, and an aromatic residue (Y161) in strand  $\beta$ 7 and thus establishing the  $\gamma$ -glutamylcyclotransferase fold for GCG1.

*Catalytic site of GCG1:-* The crystal structure of GCG1, during the refinement, consistently showed an electron density in the difference Fourier map above  $3.0$   $\sigma$  level. The electron density was modelled with a benzoic acid according to the shape of the electron density and refined further. The refinement parameters for the benzoic acid were within the limits and showed well defined electron density for it (Figure 8A). To confirm the presence of benzoic acid the GCG1 was subjected to mass spectrometric analysis as described in experimental procedures. The mass spectrometric data (data not shown) showed a peak at  $122.0823$  Da that corresponded to benzoic acid (mol. wt.  $122.12$  Da). Although we did not add any benzoic acid during purification or crystallization process, it was possible that it might originate from culture media or from trace elements present in the chemicals used for

protein purification. A similar observation was also reported in the other crystal structures (25,26). The benzoic acid is interacting with GCG1 mainly through hydrogen bond and hydrophobic interactions (Figure 8B). The O2 of benzoic acid interacts with backbone nitrogen atoms of Tyr-13. Moreover, O2 also interacts with carbonyl oxygen of Leu-11 and backbone nitrogen of Tyr-161 through a water molecule (W2). The O1 of benzoic acid interacts with backbone nitrogen atoms of Gly-14 and Leu-16. Similarly, the C3 of benzoic acid interacts with CE1 of Tyr-119 through hydrophobic interaction.

Interestingly, the crystal structure of semet-GCG1-mutant also showed electron density at the same position as benzoic acid in native GCG1 structure. However, we could model this electron density only with succinic acid (Figure 8C) as benzoic acid was not compatible with the shape of the electron density and 1M succinic acid was used for the crystallization of semet-GCG1-mutant protein. The succinic acid in the model occupies a similar position as that of benzoic acid and its interactions were also conserved (Figure 8D). The O1 of succinic acid interacts with backbone nitrogen of Gly-14, Ser-15 and Leu-16, while, O2 interacts with the backbone nitrogen of Tyr-13. In addition O2 also interacts with carbonyl oxygen of Leu-11 and backbone nitrogen of Tyr-161 through a water molecule. The O3 of succinic acid interacts with backbone nitrogen and hydroxyl group of Ser-15. It also interacts with hydroxyl group of Tyr-196. Finally the O4 of succinic acid interacts with OE1 and OE2 of Glu-115 along with hydroxyl group of Ser-15 and thus stabilizing its interaction with GCG1.

The superposition of GCG1 with  $\gamma$ -glutamylaminecyclotransferase (GGACT) (24) revealed that the benzoic acid and succinic acid occupied the same position as that of 5-oxoproline (a product of GCG1 and GGACT) in GGACT (Figure 8E). Therefore, the crystal structure of GCG1 represents the benzoic acid bound form and the site where benzoic acid is bound is presumably the catalytic site of GCG1.

*Comparison of GCG1 with other members of  $\gamma$ -glutamylcyclotransferase family:*-Although the similarity search using GCG1 sequence did not reveal any close homolog structure available in the PDB database, the similarity search using the structure of GCG1 in PDBeFOLD server (27) revealed similar structures that belong to  $\gamma$ -glutamylcyclotransferase family. The GCG1 structure showed close similarity with  $\gamma$ -glutamylcyclotransferase (PDBID: 3JUC) (28) and  $\gamma$ -glutamylaminecyclotransferase (PDBID: 3CRY) (24) with r.m.s. deviation of about 2.5Å for 135 C $^{\alpha}$  atoms (Figure 9A). However, the superposition of these structures revealed that they were similar only upto the  $\beta$ -barrel region where the  $\gamma$ -glutamyl moiety binds to the protein. Apart from this region each protein had different number of  $\alpha$ -helices and  $\beta$ -strands that decorate the  $\beta$ -barrel topology.

## DISCUSSION

The studies described here demonstrate a separate pathway in mammalian cells for constitutive, cytosolic degradation of glutathione that is mediated by the ChaC2 protein. The ChaC2 proteins were shown to specifically degrade glutathione to yield 5-oxoproline and Cys-Gly. Earlier the ChaC proteins have been grouped as one family. However, it is clear from both sequence and function, that ChaC1 and ChaC2 proteins represent distinct branches in the ChaC family. The discovery that the ChaC2 protein acts on cytosolic glutathione in a manner distinct from ChaC1 makes it the third enzyme capable of degrading glutathione in mammalian cells, the others being the ChaC1 and the  $\gamma$ -glutamyltranspeptidase enzymes. With the yeast *Saccharomyces cerevisiae* and the plant *Arabidopsis thaliana* also having multiple pathways for glutathione degradation (29), it is clear that glutathione degradation, which has till now been relatively poorly investigated has a far more important role to play in glutathione homeostasis. Studies in yeast have in fact led to conclude that glutathione degradation is the key element in glutathione homeostasis (14).

In contrast to what has been previously considered, studies on yeast have shown that glutathione degradation occurs continuously and

that glutathione has a relatively short half-life. Under stress conditions, glutathione was found to be turned over rapidly with a half-life of 60 minutes, but surprisingly, even under un-stressed conditions glutathione was turned over with a half-life of about 90 minutes (14). The human and mouse ChaC2 proteins described are likely to participate in a similar continuous and constant, housekeeping function of glutathione degradation in mammalian cells.

Lower eukaryotes and especially the unicellular eukaryotes have only a single ChaC member. Sequence and functional evaluation indicated that the single ChaC member in these lower eukaryotes are orthologous to the low efficiency ChaC2 protein. Thus, it is likely that the ChaC2 enzyme involved in constitutive, low level turnover is the ancestral enzyme, while the ChaC1 proteins present exclusively in higher eukaryotes might have evolved with higher catalytic efficiency for carrying out acute glutathione turnover required under stress conditions.

Despite their importance in maintaining glutathione homeostasis, no structural information hitherto is available for any member of the ChaC family proteins. Therefore, to gain mechanistic insights into the functioning of ChaC family we have determined the crystal structure of GCG1 from yeast, a ChaC2 homologue at 1.34 Å resolution. The crystal structure of GCG1 reveals a  $\gamma$ -glutamyl cyclotransferase-like fold in spite of its low sequence similarity.

Earlier studies with  $\gamma$ -glutamyl cyclotransferase (24) have proposed a Glu residue to act as a general acid/base, where the  $\alpha$ -amino group of L- $\gamma$ -glutamyl moiety of the substrate is deprotonated by the Glu followed by nucleophilic attack of this amine onto the side chain amide carbon atom leading to formation of an oxyanion intermediate. This oxyanion eventually collapses to form 5-oxoproline. The protonated Glu donates a hydrogen ion to the amine of the  $\alpha$ -linked amino portion of the substrate. We speculate that the GCG1 will also follow the same catalytic mechanism to convert the glutathione into 5-oxoproline and Cys-Gly

peptide, as the Glu residue (corresponding to Glu-115 in GCG1) is conserved throughout the ChaC family (Figure 9B). Importantly, the mutation of E115A in GCG1 completely abolished its catalytic activity (10). Notably, the recently identified Botch (30), that is identical to mouse ChaC1 has been shown to possess a  $\gamma$ -glutamylcyclotransferase activity that acts on the Notch protein. However, the glutamate on a protein does not have a free  $\alpha$ -amino group that is required for deprotonation and thus the mechanism of Notch inactivation is yet unknown and needs to be established.

To understand the differential catalytic efficiency shown by ChaC2 as compared to ChaC1 we compared the sequence of ChaC1 with the GCG1 sequence and structure. The GCG1 structure, while it shows structural similarity with other  $\gamma$ -glutamylcyclotransferase family proteins, this similarity is extended only upto the  $\beta$ -barrel topology and a  $\alpha$ -helix, a conserved region across all members of this family (Figure 9A). The other secondary structures and loops beyond this  $\beta$ -barrel topology are not conserved and may contribute to the specificity and possible differences in catalytic efficiency of the two proteins. In addition, apart from small sequence variations between ChaC1 and ChaC2 an initial N-terminal region of about 25 amino acids are missing in the ChaC2 and other ChaC proteins compared to ChaC1 (Figure 9B). This region may partly contribute to higher catalytic efficiency shown by ChaC1. However, the contribution of other residues that vary between ChaC1 and ChaC2 are not ruled out and further experiments are required to determine their role in displaying different catalytic efficiencies.

Interestingly, the crystal structure of native GCG1 and semet-GCG1-mutant clearly shows an additional electron density at the catalytic site that could be modelled as benzoic acid and succinic acid respectively. Although, the interactions of these two ligands with the protein are largely conserved (Figure 8B and 8E), the superposition of these two structures reveal a conformational change observed in a loop (Loop1) formed by the residues 110-YLNVREQNGY-119 (Figure 9C). Based on this



observed conformational change we propose that the 'Loop1' of GCG1 may play a role in acquiring its specificity. However, additional experiments and GCG1 structures along with substrate are required to validate our prediction.

In summary, we have demonstrated that the ChaC2 protein of mammals and its orthologue in lower eukaryotes and prokaryotes is responsible for the continuous, but basal turnover of cytosolic glutathione and thus it represents an additional pathway in glutathione degradation.

## EXPERIMENTAL PROCEDURES:

**Chemicals and reagents:-** All the chemicals and reagents used were either analytical grade or molecular biology grade. Gel extraction kit, plasmid preparation kits, Ni-NTA resins were obtained from Qiagen. Oligonucleotides were synthesised from Sigma and IDT. All the media components were obtained from Difco. Glutathione, cysteine, ninhydrin, methionine, sorbitol and GSSG were obtained from Sigma. Amplex red kit for glutamate estimation was obtained from Roche. Restriction enzymes, Vent DNA polymerase and other DNA modifying enzymes were obtained from New England Biolabs. PAGE protein markers were obtained from MBI Fermentas.

**Strains, media and growth conditions:-** *E. coli* DH5 $\alpha$  was used as a cloning host and BL21, BL21 DE3 pLysS and BL21 Rosetta were used as an expression host. The *Saccharomyces cerevisiae* ABC1723 (*MAT $\alpha$  his3 $\Delta$ 1 leu2 $\Delta$ 0 lys2 $\Delta$ 0 met15 $\Delta$ 0 ura3 $\Delta$ 0 ecm38 $\Delta$ ::KanMX4 dug3*), ABC 1195 (*MAT $\alpha$  his3 $\Delta$ 1 lys2 $\Delta$ 0 met15 $\Delta$ 0 ura3 $\Delta$ 0 gsh1  $\Delta$ ::leu2*) and BY4741 (*MAT $\alpha$  his3 $\Delta$ 1 leu2 $\Delta$ 0 met15 $\Delta$ 0 ura3 $\Delta$ 0*) were used for genetic complementation, ROS and glutathione assays respectively. The yeast strains were maintained at YPD (yeast extract, peptone and Dextrose). For genetic complementation assays synthetic defined (SD) minimal media containing YNB, ammonium sulphate and dextrose supplemented with histidine, leucine, lysine and methionine (80mg/l) were used. Glutathione was used at a concentration of

300 $\mu$ M. Yeast transformations were carried out using lithium acetate method (31).

**Cell culture:-** Cell lines were obtained from NCCS-Pune and maintained in DMEM and RPMI-1640 supplemented with 10% fetal bovine serum, penicillin (100units/ml), and streptomycin (100 $\mu$ g/ml; Invitrogen Corp.) at 37°C in a humidified atmosphere with 5% CO<sub>2</sub>.

**Bioinformatics analysis:-** Human ChaC2 and ChaC1 sequences were obtained from the NCBI database and analysed for homologues in different organisms using BLASTp (31). Multiple sequence analysis was performed using T-coffee software (32). The multiple sequence data file was then used to obtain a neighbour joining based phylogenetic tree with MEGA6 software (33).

**Cloning and expression of human ChaC1, human/mouse ChaC2, E. coli ChaC, yeast GCG1 and semet-GCG1-mutant proteins:-** The human ChaC1/ChaC2 and mouse ChaC2 genes were PCR amplified from cDNA clones that were obtained from SAF labs and subcloned into the yeast expression vector p416TEF using primers as mentioned in Table 1. The genes were cloned at the *Bam*H1 and *Xho*I sites. Additionally, the mouse ChaC2, human ChaC2 and yeast GCG1 were PCR amplified using C-terminal 8XHis tag reverse primer and cloned in the pET23d vector. Similarly, the *E. coli* ChaC (amplified from *E. coli* genomic DNA), yeast GCG1-mutant (S42M, L77M, A141M and V176M) and human ChaC1 were cloned in pET23a vector. For the expression of proteins the constructs carrying the mouse ChaC2, human ChaC2, human ChaC1, yeast GCG1, GCG1-mutant and *E. coli* ChaC were transformed in *E. coli* BL21 (DE3), *E. coli* BL21 Rosetta, *E. coli* BL21 (DE3) pLysS, *E. coli* BL21 (DE3), *E. coli* BL21 Rosetta and *E. coli* BL21 (DE3) pLysS respectively.

For the expression of proteins in *E. coli*, the primary cultures were grown overnight in LB media containing ampicillin (100  $\mu$ g/ml). Chloramphenicol (35  $\mu$ g/ml) was also added when *E. coli* strains carried dual selection. The secondary cultures bearing the mouse ChaC2,

human ChaC1/ChaC2 and yeast GCG1 (10) clones were inoculated at 0.05 OD<sub>600nm</sub> and allowed to grow till the OD<sub>600nm</sub> reached 0.5-0.6 (1 OD<sub>600nm</sub> = 2x10<sup>7</sup> cells). The cultures were induced with 0.5 mM IPTG and kept at 18°C for 16 hrs. For *E. coli* ChaC, the protocol was slightly modified because majority of the *E. coli* ChaC protein entered into inclusion bodies. Therefore, the secondary culture was allowed to grow till 0.3 OD<sub>600nm</sub> and 3% ethanol was added to the culture along with 0.5 mM IPTG. The culture was then allowed to grow at 18°C with 180 rpm for 15 hrs. For the expression and labelling of GCG1-mutant with selenomethionine (semet-GCG1-mutant), a single colony carrying pET23a-GCG1-mutant was inoculated in 50ml of minimal media (Molecular Dimensions, UK) containing L-methionine supplemented with 100µg/ml ampicillin and 35µg/ml chloramphenicol and incubated at 37°C for 16 hrs. The overnight grown culture was harvested, the pellet was washed thrice with distilled water and finally resuspended in 1 ml of water. The resuspended pellet was inoculated in 500 ml of pre-warmed minimal media containing L-selenomethionine. The cells were grown till the OD<sub>600nm</sub> reached a value of 0.5 followed by the addition 0.1 M sorbitol and 0.1 mM IPTG and the cells were grown further for 16 hrs at 16°C. All the cells were harvested by spinning the culture at 10000 rpm for 10 min at 4°C.

*Purification of human ChaC1, human/mouse ChaC2, E. coli ChaC, yeast GCG1 and semet-GCG1-mutant proteins:-* The harvested cell pellets were lysed by sonication in a buffer containing 50 mM Tris pH 8, 300 mM NaCl and 1 mM PMSF. The cell lysates were centrifuged at 15000 g for 1 hr at 4°C and the supernatant obtained was loaded over Ni-NTA columns which were pre-equilibrated with 50 mM Tris pH 8.0, 300 mM NaCl buffer (Buffer A). The Ni-NTA columns were washed with 5 column volumes of buffer A containing 20 mM imidazole. The bound proteins were eluted in buffer A containing 200-250 mM imidazole and dialyzed overnight against 50 mM Tris pH 8.0, 300 mM NaCl using 10 kDa cutoff membrane except yeast GCG1 and semet-GCG1-mutant which were dialysed with 100 mM Tris and 200

mM NaCl. The GCG1 and semet-GCG1-mutant proteins were further purified by gel filtration chromatography using pre-packed Sephacryl S-200 column (16/600 mm, GE Healthcare, USA) that was pre-equilibrated with 100 mM Tris pH 8.0, 200 mM NaCl buffer. In addition, the gel filtration chromatography using pre-packed superdex 200 column (10/300 mm) (GE Healthcare, USA) was also carried out to estimate the molecular weight and oligomeric nature of Ni-NTA purified human ChaC1, human ChaC2, mouse ChaC2 and *E. coli* ChaC proteins. The peaks obtained were analysed against standard curve that was established using protein standards (GE Healthcare, USA). The purity of proteins were checked by SDS-PAGE and the concentration of proteins were estimated by the Bradford method (34) at each step of purification.

*In vivo functional complementation assays in S. cerevisiae:-* The transformants were grown overnight in SD medium containing methionine or glutathione. Primary culture was used to inoculate secondary culture and allowed to grow till 0.6 OD<sub>600nm</sub>. The cells were harvested, washed and diluted in sterile water at 0.2 OD<sub>600nm</sub>. Serial dilutions were then made and 10 µl of cell suspension was spotted on plates containing SD medium with or without glutathione.

*Assay of  $\gamma$ -glutamylcyclotransferase activity on glutathione,  $\gamma$ -Glu-Cys using Dug1p-coupled assay:-* Glutathione degradation activity of ChaC2 proteins were performed using Dug1 coupled assay as described earlier (10). 5 µg of human ChaC2, 2.5 µg of mouse ChaC2 and 10 µg of *E. coli* ChaC were incubated with 0.2 mM to 15 mM GSH in 50 µl of reaction mix containing 50 mM Tris pH 8 and 5 mM DTT for 30 min at 37°C. The reaction was terminated thereafter by heating at 95°C for 5 min. 5 µg of recombinant Dug1p and 20 µM MnCl<sub>2</sub> was added to each reaction and incubated further for 1hr at 37°C. Cysteine release was estimated using ninhydrin based method (35). The kinetic parameters were obtained by plotting data using graph pad prism 5 software.

*Assay of  $\gamma$ -glutamylcyclotransferase activity on GSSG and glutathione using 5-oxoprolinase coupled assay:-*The activity against GSSG was checked by measuring the 5-oxoprolinase released during the reaction using 2.5  $\mu$ g of human ChaC2 and human ChaC1 proteins. The 5-oxoprolinase was estimated using 5-oxoprolinase coupled assay as described earlier (10).

*Determination of intracellular ROS generation:-* Intracellular ROS generation was assessed using 5-(and-6)-chloromethyl-2,7-dichlorodihydrofluorescein diacetate, (CM-H<sub>2</sub>DCFDA) (Molecular Probes). WT yeast cells ABC1195 transformed with human ChaC1 and human ChaC2 cloned in p416TEF expression vector were grown in minimal media containing 10  $\mu$ M glutathione. 0.8 OD<sub>600nm</sub> cells were pelleted, washed and loaded with CM-H<sub>2</sub>DCFDA (10  $\mu$ M) for 30 minutes. Cells were washed with PBS and fluorescence (excitation 493 nm, emission 527 nm) was then measured. To confirm that DCF was able to detect increased oxidative stress, cells in control medium were treated with 100  $\mu$ M H<sub>2</sub>O<sub>2</sub> and it was taken as positive control. Confocal microscopy was also done to show dose-dependent changes in DCF levels in cells exposed to H<sub>2</sub>O<sub>2</sub>. Cells were plated onto poly-L-lysine-coated coverslips and were loaded with CM-H<sub>2</sub>DCFDA (10  $\mu$ M) 30 min. After fixing with 4% paraformaldehyde, cells were washed with PBS and mounted using Vectashield mounting medium and stored at 4°C in dark until imaging. Data was normalized to values obtained from normoxic controls.

*Determination of intracellular glutathione levels:-* The *S. cerevisiae* BY4741 strains transformed with different plasmids were grown to an O.D<sub>600nm</sub> of 0.6-0.8, harvested and resuspended to an O.D<sub>600nm</sub> of 10. Cells were lysed in 800  $\mu$ l of KPE buffer (0.1 M potassium phosphate buffer and 5 mM EDTA, pH 7.5) containing 0.6% sulfosalicylic acid and 0.1% triton X-100 using glass bead lysis method. The supernatant was used for the estimation of glutathione by DTNB method according to the protocol by Rahman et al (36).

*RNA isolation and Quantitative real-time PCR:-* Cultured cells were exposed to sulphur stress by growing in sulphur and cysteine free DMEM for different time periods. Total RNA was extracted using an RNeasy kit (Qiagen) and quantified using a spectrophotometer at 260 nm. 500 ng of total RNA was reverse-transcribed to cDNA using a Superscript II kit (Takara) with oligo (dT) primer. In the real-time PCR step, PCR reactions were performed in triplicates with 1  $\mu$ L cDNA/20  $\mu$ L reaction and primers specific for human ChaC1 and human ChaC2 using SYBR Premix ExTaq in an Eppendorf RealPlex Mastercycler. Thermal cycling was initiated at 94°C for 30 sec followed by 40 cycles of PCR (94°C for 5 s and 68°C for 30 s).  $\beta$ -actin was used as an endogenous control. The Ct method was applied to normalize expression relative to the actin gene.

*Western blot analysis:-* For Western blot analysis cells were lysed in buffer containing 150 mM NaCl, 1.0% Triton X-100, 0.5% sodium deoxycholate, 0.1% SDS and 50 mM Tris (pH 8.0). Protein concentration was estimated by the Bradford reagent. Proteins (50  $\mu$ g) were electrophoresed on a 15% SDS-polyacrylamide gel and transferred to nitrocellulose membrane (Millipore). The membrane was blocked with 5% BSA and probed with monoclonal antibody to ChaC1 (Cat# AV42623, Sigma Chemical Co.) and ChaC2 (Cat# SAB2104121, Sigma Chemical Co.) at 1: 750 dilutions, incubated at 4°C overnight, followed by incubation with secondary antibody for 2 hrs at 37°C. Immunoreactive bands were visualized using the enhanced chemiluminescence detection system (Amersham) following the manufacturer's protocol.

*Immunocytochemistry for in vivo localization:-* Cultured cells were plated onto poly-L-lysine-coated coverslips and fixed with 4% paraformaldehyde after exposing cells for 48 hrs to tunicamycin. Cells were blocked with 5% BSA and then incubated with monoclonal antibody to ChaC2 (1: 100; Sigma), at 4°C for overnight and then incubated in goat anti-rabbit Alexa Fluor 488 (1:20000; Invitrogen) for 30 min. For control, primary antibody was not

added in above treatment. After washing in PBS, slides were mounted using Vectashield mounting medium and stored at 4°C in dark until imaging. Images were captured using confocal microscope (Zeiss LSM 780).

*Mass spectrometry analysis of the purified protein:*- The purified GCG1 protein used for crystallographic studies was subjected to mass spectrometric analysis to confirm the presence of bound benzoic acid with the purified protein. The intact protein mass was analyzed using WATERS SYNAPT G2S QTOF mass spectrophotometer in ESI positive mode. The mass range and scan rate were set to record m/z from 50 to 2000 Daltons in resolution mode. The sample was directly infused with a flow rate of 100 µl/min, capillary voltage of 3 KV, cone voltage of 25 V at 120°C source temperature and dissolution temperature of 350°C. Raw data obtained was analyzed using mass lynx software.

*Crystallization, data collection and structure determination of GCG1:*- The yeast ChaC2 homolog, GCG1 (20 mg/ml) and semet-GCG1-mutant (12 mg/ml) in 100 mM Tris pH 8.0, 200 mM NaCl were used to setup various commercial crystallization screens by sitting drop vapour diffusion method with 96 well plates (Molecular Dimensions, UK). Each protein drop with 1 µl of protein and 1 µl of precipitant was equilibrated against 60 µl of reservoir solution followed by incubation at 20°C. The good quality crystals for native GCG1 were appeared in 0.2 M ammonium phosphate, 20% PEG 3350, pH 4.7 and 15% glycerol, after seeding. For semet-GCG1-mutant, quality crystals were obtained in 1M succinic acid pH 7.0, 0.1 M HEPES pH 7.0 and 1% w/v PEG-MME 2000, after seeding.

The X-ray diffraction data for native GCG1 and semet-GCG1-mutant were collected using synchrotron radiation available at BM14 beamline (European Synchrotron Radiation Facility (ESRF), Grenoble, France) equipped with MAR Mosaic CCD detector. The semet-GCG1-mutant crystal was soaked in 20% (v/v) glycerol in mother liquor for 10 sec and immediately flash cooled in liquid nitrogen prior

to data collection. Total 991 images were collected for semet-GCG1-mutant crystal at wavelength of 0.9787 Å. For native GCG1, the glycerol (15%) used in crystallization experiment was sufficient for cryoprotection and therefore the crystal was directly flash cooled in liquid nitrogen. A total of 2000 images were collected for native GCG1 at wavelength of 0.9763 Å. Both the datasets were indexed, integrated and scaled using HKL2000 (37) suite of programs.

The crystal structure of semet-GCG1-mutant was solved by single wavelength anomalous diffraction (SAD) method using AUTOSOL as implemented in PHENIX (37). Initially, four out of seven selenium atoms (at residue number 42, 141, 176 and 207) were located. The other three selenium atoms anticipated at residue number 1, 77 and 210 were not located by the program. Moreover, refining these residues as selenomethionine at these positions did not fit well and therefore these residues were refined as methionine only. The incomplete incorporation of selenomethionine in the protein may be due to the usage of non methionine-auxotrophic strain for the expression of semet-GCG1-mutant protein. Nevertheless, the initial phases obtained from four selenium atoms were improved by density modification and the modified map showed an excellent electron density. Using the modified map the automatic model building was able to build around 200 residues out of 232 residues. Further refinement and model building were carried out in PHENIX and COOT (37,38) respectively. The three dimensional structure thus obtained for the semet-GCG1-mutant was used as a template for the structure determination of native GCG1 by molecular replacement method using PHASER (39) as implemented in CCP4 (40) suite. The PHASER with default parameters gave a single solution with two molecules in the asymmetric unit. Further refinement was done using rigid body and restrained refinement using REFMAC5 (41) followed by refinement in PHENIX. The manual model building was done using COOT. The GCG1 model was subjected to simulating annealing refinement using PHENIX for further improvement and to minimize any model bias. All the atoms were

refined with anisotropic temperature factors. The model building and refinement were carried out

iteratively until the  $R_{\text{work}}$  and  $R_{\text{free}}$  were converged.

**Acknowledgements:** AKB acknowledges financial assistance from Department of Science & Technology, Government of India (Project No: SB/SO/BB/017/2014). AKB is recipient of a JC Bose national fellowship from Department of Science & Technology, Government of India. A. Kaur and RS are recipients of University Grants Commission senior research fellowship; AC and AK are recipients of a senior research fellowship from Council of Scientific and Industrial Research (CSIR), Government of India. RG is recipient of senior research fellowship from Indian Council of Medical Research, Government of India. We thank the EMBL staff Dr Hassan Belrhali and Dr. Babu A. Manjasetty for providing support on the beamline and EMBL-DBT for providing access to the BM14 beamline at the ESRF. We also thank Department of Biotechnology, Government of India for providing financial assistance to RG for collecting data at BM14. SK acknowledges support by CSIR through network project BSC-104.

**Conflict of interest:** The authors declare that they have no conflicts of interest with the content of this article.

**Author contributions:** A. Kaur had purified and characterized both the human enzymes and made the mutants. AC had performed the *in vivo* experiments. RG and RS performed the experiments related to purification, crystallization, data collection and structure analysis of GCG1. SK supervised the analysis and structural characterization of GCG1. AKB analysed and supervised the experiments related to enzyme characterization and *in vivo* experiments. All authors contributed in writing and preparation of the manuscript.

**Deposition of coordinates with Protein Data Bank:** The atomic coordinates and structure factors for semet-GCG1-mutant (5HWI) and GCG1-benzoic acid complex (5HWK) have been deposited in the Protein Data Bank (<http://www.pdb.org>).

## REFERENCES

1. Fahey, R. C., Newton, G. L., Arrick, B., Overdank-Bogart, T., and Aley, S. B. (1984) *Entamoeba histolytica*: a eukaryote without glutathione metabolism. *Science* **224**, 70-72
2. Meister, A., and Anderson, M. E. (1983) Glutathione. *Annual review of biochemistry* **52**, 711-760
3. Penninckx, M. J., and Elskens, M. T. (1993) Metabolism and functions of glutathione in microorganisms. *Advances in microbial physiology* **34**, 239-301
4. Arthur, J. R. (2000) The glutathione peroxidases. *Cellular and molecular life sciences : CMLS* **57**, 1825-1835
5. Hayes, J. D., Flanagan, J. U., and Jowsey, I. R. (2005) Glutathione transferases. *Annual review of pharmacology and toxicology* **45**, 51-88
6. Dalle-Donne, I., Rossi, R., Colombo, G., Giustarini, D., and Milzani, A. (2009) Protein S-glutathionylation: a regulatory device from bacteria to humans. *Trends in biochemical sciences* **34**, 85-96
7. Winkler, A., Njalsson, R., Carlsson, K., Elgadi, A., Rozell, B., Abraham, L., Ercal, N., Shi, Z. Z., Lieberman, M. W., Larsson, A., and Norgren, S. (2011) Glutathione is essential for early embryogenesis--analysis of a glutathione synthetase knockout mouse. *Biochem Biophys Res Commun* **412**, 121-126
8. Franco, R., and Cidlowski, J. A. (2009) Apoptosis and glutathione: beyond an antioxidant. *Cell Death Differ* **16**, 1303-1314
9. Townsend, D. M., Tew, K. D., and Tapiero, H. (2003) The importance of glutathione in human disease. *Biomed Pharmacother* **57**, 145-155
10. Kumar, A., Tikoo, S., Maity, S., Sengupta, S., Sengupta, S., Kaur, A., and Bachhawat, A. K. (2012) Mammalian proapoptotic factor ChaC1 and its homologues function as  $\gamma$ -glutamyl cyclotransferases acting specifically on glutathione. *EMBO reports* **13**, 1095-1101
11. Kumar, C., Igarria, A., D'autreaux, B., Planson, A. G., Junot, C., Godat, E., Bachhawat, A. K., Delaunay-Moisan, A., and Toledano, M. B. (2011) Glutathione revisited: a vital function in iron metabolism and ancillary role in thiol-redox control. *The EMBO journal* **30**, 2044-2056
12. Srikanth, C. V., Vats, P., Bourbouloux, A., Delrot, S., and Bachhawat, A. K. (2005) Multiple cis-regulatory elements and the yeast sulphur regulatory network are required for the regulation of the yeast glutathione transporter, Hgt1p. *Current genetics* **47**, 345-358
13. Rajasekaran, N. S., Connell, P., Christians, E. S., Yan, L.-J., Taylor, R. P., Orosz, A., Zhang, X. Q., Stevenson, T. J., Peshock, R. M., and Leopold, J. A. (2007) Human  $\alpha$ B-crystallin mutation causes oxido-reductive stress and protein aggregation cardiomyopathy in mice. *Cell* **130**, 427-439
14. Baudouin-Cornu, P., Lagniel, G., Kumar, C., Huang, M. E., and Labarre, J. (2012) Glutathione degradation is a key determinant of glutathione homeostasis. *The Journal of biological chemistry* **287**, 4552-4561
15. Tate, S. S., and Meister, A. (1981) gamma-Glutamyl transpeptidase: catalytic, structural and functional aspects. *Mol Cell Biochem* **39**, 357-368
16. Kaur, H., Kumar, C., Junot, C., Toledano, M. B., and Bachhawat, A. K. (2009) Dug1p Is a Cys-Gly peptidase of the gamma-glutamyl cycle of *Saccharomyces cerevisiae* and represents a novel family of Cys-Gly peptidases. *The Journal of biological chemistry* **284**, 14493-14502
17. Ganguli, D., Kumar, C., and Bachhawat, A. K. (2007) The alternative pathway of glutathione degradation is mediated by a novel protein complex involving three new genes in *Saccharomyces cerevisiae*. *Genetics* **175**, 1137-1151
18. Mungrue, I. N., Pagnon, J., Kohannim, O., Gargalovic, P. S., and Lulis, A. J. (2009) CHAC1/MGC4504 is a novel proapoptotic component of the unfolded protein response, downstream of the ATF4-ATF3-CHOP cascade. *The Journal of Immunology* **182**, 466-476

19. Crawford, R. R., Prescott, E. T., Sylvester, C. F., Higdon, A. N., Shan, J., Kilberg, M. S., and Mungrue, I. N. (2015) Human CHAC1 Protein Degrades Glutathione, and mRNA Induction Is Regulated by the Transcription Factors ATF4 and ATF3 and a Bipartite ATF/CRE Regulatory Element. *The Journal of biological chemistry* **290**, 15878-15891
20. Fujiwara, S., Kawazoe, T., Ohnishi, K., Kitagawa, T., Popa, C., Valls, M., Genin, S., Nakamura, K., Kuramitsu, Y., and Tanaka, N. (2016) RipAY, a Plant Pathogen Effector Protein, Exhibits Robust  $\gamma$ -Glutamyl Cyclotransferase Activity When Stimulated by Eukaryotic Thioredoxins. *Journal of Biological Chemistry* **291**, 6813-6830
21. Kantardjieff, K. A., and Rupp, B. (2003) Matthews coefficient probabilities: Improved estimates for unit cell contents of proteins, DNA, and protein-nucleic acid complex crystals. *Protein Sci* **12**, 1865-1871
22. Brunger, A. T. (1992) Free R value: a novel statistical quantity for assessing the accuracy of crystal structures. *Nature* **355**, 472-475
23. Krissinel, E., and Henrick, K. (2007) Inference of macromolecular assemblies from crystalline state. *Journal of molecular biology* **372**, 774-797
24. Oakley, A. J., Coggan, M., and Board, P. G. (2010) Identification and Characterization of  $\gamma$ -Glutamylamine Cyclotransferase, an Enzyme Responsible for  $\gamma$ -Glutamyl- $\epsilon$ -lysine Catabolism. *Journal of Biological Chemistry* **285**, 9642-9648
25. Steegborn, C., Danot, O., Huber, R., and Clausen, T. (2001) Crystal structure of transcription factor MalT domain III: a novel helix repeat fold implicated in regulated oligomerization. *Structure* **9**, 1051-1060
26. Hwang, J., Nguyen, L. T., Jeon, Y. H., Lee, C. Y., and Kim, M. H. (2015) Crystal structure of fully oxidized human thioredoxin. *Biochemical and biophysical research communications* **467**, 218-222
27. Krissinel, E., and Henrick, K. (2004) Secondary-structure matching (SSM), a new tool for fast protein structure alignment in three dimensions. *Acta Crystallographica Section D: Biological Crystallography* **60**, 2256-2268
28. Oakley, A. J., Yamada, T., Liu, D., Coggan, M., Clark, A. G., and Board, P. G. (2008) The identification and structural characterization of C7orf24 as  $\gamma$ -glutamyl cyclotransferase an essential enzyme in the  $\gamma$ -glutamyl cycle. *Journal of Biological Chemistry* **283**, 22031-22042
29. Kumar, S., Kaur, A., Chattopadhyay, B., and Bachhawat, A. K. (2015) Defining the cytosolic pathway of glutathione degradation in Arabidopsis thaliana: role of the ChaC/GCG family of  $\gamma$ -glutamyl cyclotransferases as glutathione-degrading enzymes and AtLAP1 as the Cys-Gly peptidase. *Biochemical Journal* **468**, 73-85
30. Chi, Z., Byrne, S. T., Dolinko, A., Harraz, M. M., Kim, M. S., Umanah, G., Zhong, J., Chen, R., Zhang, J., Xu, J., Chen, L., Pandey, A., Dawson, T. M., and Dawson, V. L. (2014) Botch is a gamma-glutamyl cyclotransferase that deglycinates and antagonizes Notch. *Cell Rep* **7**, 681-688
31. Ito, H., Fukuda, Y., Murata, K., and Kimura, A. (1983) Transformation of intact yeast cells treated with alkali cations. *Journal of bacteriology* **153**, 163-168
32. Notredame, C., Higgins, D. G., and Heringa, J. (2000) T-Coffee: A novel method for fast and accurate multiple sequence alignment. *Journal of molecular biology* **302**, 205-217
33. Tamura, K., Stecher, G., Peterson, D., Filipski, A., and Kumar, S. (2013) MEGA6: Molecular Evolutionary Genetics Analysis version 6.0. *Molecular biology and evolution* **30**, 2725-2729
34. Bradford, M. M. (1976) A rapid and sensitive method for the quantitation of microgram quantities of protein utilizing the principle of protein-dye binding. *Anal Biochem* **72**, 248-254
35. Gaitonde, M. (1967) A spectrophotometric method for the direct determination of cysteine in the presence of other naturally occurring amino acids. *Biochemical Journal* **104**, 627
36. Rahman, I., Kode, A., and Biswas, S. K. (2006) Assay for quantitative determination of glutathione and glutathione disulfide levels using enzymatic recycling method. *Nature protocols* **1**, 3159-3165

37. Adams, P. D., Afonine, P. V., Bunkoczi, G., Chen, V. B., Davis, I. W., Echols, N., Headd, J. J., Hung, L. W., Kapral, G. J., Grosse-Kunstleve, R. W., McCoy, A. J., Moriarty, N. W., Oeffner, R., Read, R. J., Richardson, D. C., Richardson, J. S., Terwilliger, T. C., and Zwart, P. H. (2010) PHENIX: a comprehensive Python-based system for macromolecular structure solution. *Acta Crystallogr D Biol Crystallogr* **66**, 213-221
38. Emsley, P., and Cowtan, K. (2004) Coot: model-building tools for molecular graphics. *Acta Crystallographica Section D: Biological Crystallography* **60**, 2126-2132
39. McCoy, A. J., Grosse-Kunstleve, R. W., Adams, P. D., Winn, M. D., Storoni, L. C., and Read, R. J. (2007) Phaser crystallographic software. *J Appl Crystallogr* **40**, 658-674
40. Winn, M. D., Ballard, C. C., Cowtan, K. D., Dodson, E. J., Emsley, P., Evans, P. R., Keegan, R. M., Krissinel, E. B., Leslie, A. G., McCoy, A., McNicholas, S. J., Murshudov, G. N., Pannu, N. S., Potterton, E. A., Powell, H. R., Read, R. J., Vagin, A., and Wilson, K. S. (2011) Overview of the CCP4 suite and current developments. *Acta Crystallogr D Biol Crystallogr* **67**, 235-242
41. Murshudov, G. N., Skubak, P., Lebedev, A. A., Pannu, N. S., Steiner, R. A., Nicholls, R. A., Winn, M. D., Long, F., and Vagin, A. A. (2011) REFMAC5 for the refinement of macromolecular crystal structures. *Acta Crystallogr D Biol Crystallogr* **67**, 355-367
42. Schrödinger, L. The PyMOL Molecular Graphics System. 1.2r3pre Ed.
43. Robert, X., and Gouet, P. (2014) Deciphering key features in protein structures with the new ENDscript server. *Nucleic Acids Res* **42**, W320-324





**TABLE 2:** Data collection and refinement statistics

	Semet-GCG1-mutant	GCG1-benzoic acid complex
<b>Data collection</b>	Se SAD	
Resolution range (Å)	50.00-1.75 (1.78-1.75) <sup>a</sup>	50.00-1.34 (1.39-1.34)
Space group	P4 <sub>2</sub> 2 <sub>1</sub> 2	P1
Unit cell parameters		
a, b, c (Å)	110.55, 110.55, 42.59	41.78, 62.02, 61.70
α, β, γ (°)	90.00, 90.00, 90.00	113.71, 89.89, 101.80
Total no. of reflections	907878	1049615
Unique reflections	25966	103046
Mosaicity range (°)	0.5-0.7	0.7-1.1
$R_{\text{merge}}^b$	0.10 (0.93)	0.08 (0.84)
Overall $I/\sigma(I)$	41.9 (2.1)	23.6 (2.0)
Completeness (%)	96.3 (76.5)	84.5 (32.3)
Redundancy	34.9 (15.2)	10.2 (6.0)
$R_{\text{pim}}^c$	0.02 (0.23)	0.03 (0.33)
CC <sub>1/2</sub>	0.99 (0.96)	0.96 (0.83)
<b>Refinement</b>		
Resolution (Å)	37.40-1.75	30.14-1.34
No. reflections	25799	103046
$R_{\text{work}} / R_{\text{free}}$	0.17 / 0.21	0.16 / 0.19
R.m.s. deviations		
Bond lengths (Å)	0.015	0.012
Bond angles (°)	1.21	1.18
Ramachandran plot, residues in		
Most favoured region (%)	99.56	97.95
Additionally allowed region (%)	0.44	2.05
Number of residues	229 (out of 232)	445 (out of 464)
Ligand name (number)	Succinic acid (1)	Benzoic acid (2)
Ion name (number)	-	Phosphate (2)
Number of atoms in		
Protein	1835	3526
Ligand/ion	8/0	18/10
Solvent molecules	142	441
B-factors (Å <sup>2</sup> )		
Wilson factor	25.03	20.58
Protein	35.96	33.11
Ligand/phosphate ion	29.74	23.95/22.12
Solvent molecules	49.23	48.96
PDBID	5HWI	5HWK

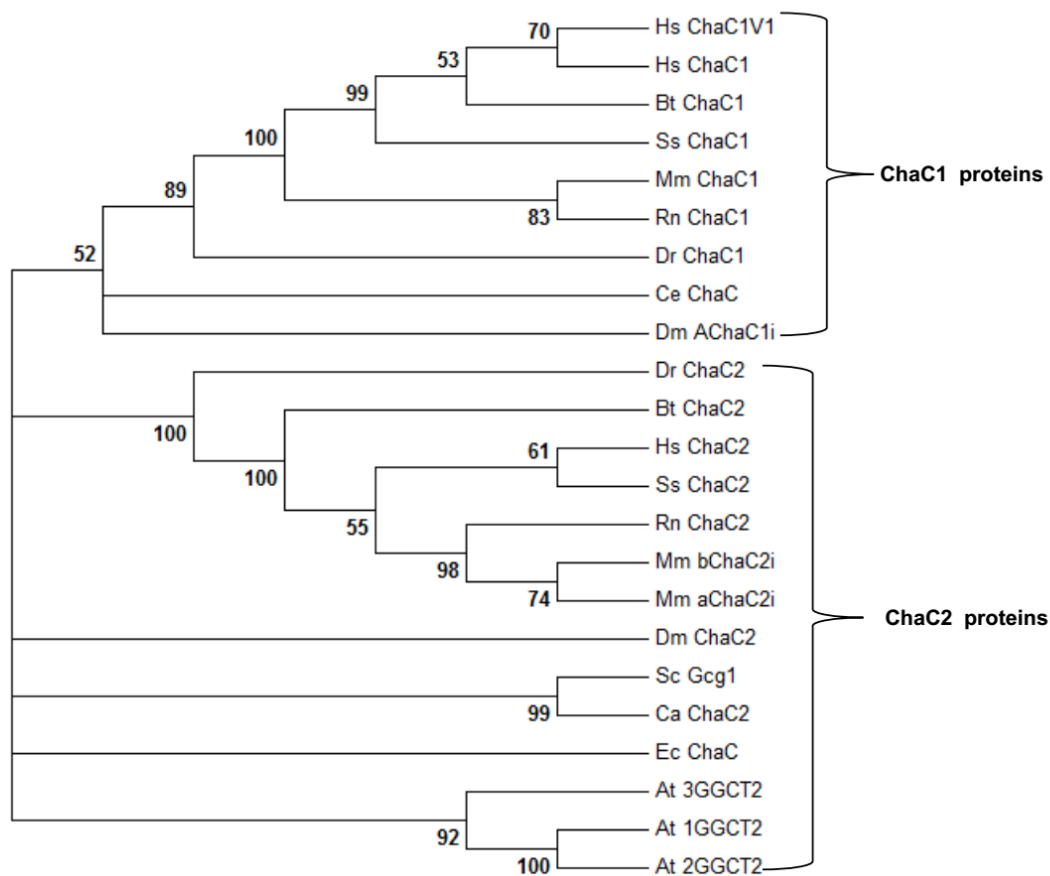
Single crystal was used for collecting each dataset.

<sup>a</sup>Values in parentheses are for highest-resolution shell.

<sup>b</sup> $R_{\text{merge}} = \frac{\sum_{hkl} \sum_i |I_i(hkl) - \langle I(hkl) \rangle|}{\sum_{hkl} \sum_i I_i(hkl)}$ , where  $I(hkl)$  is the intensity of reflection  $hkl$

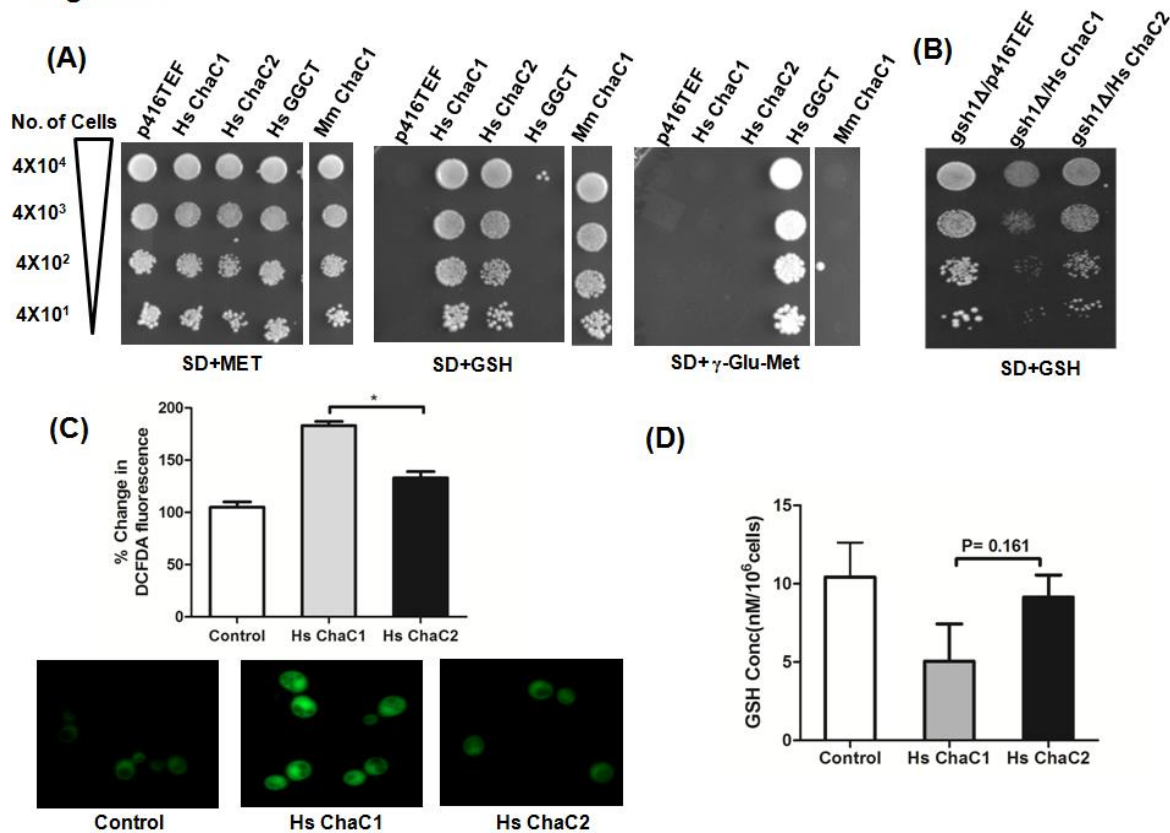
<sup>c</sup> $R_{\text{pim}} = \frac{\sum_{hkl} [n/(n-1)]^{1/2} \sum_i |I_i(hkl) - \langle I(hkl) \rangle|}{\sum_{hkl} \sum_i I_i(hkl)}$ , where  $n$  is the multiplicity, other variables as defined for  $R_{\text{merge}}$

Figure 1

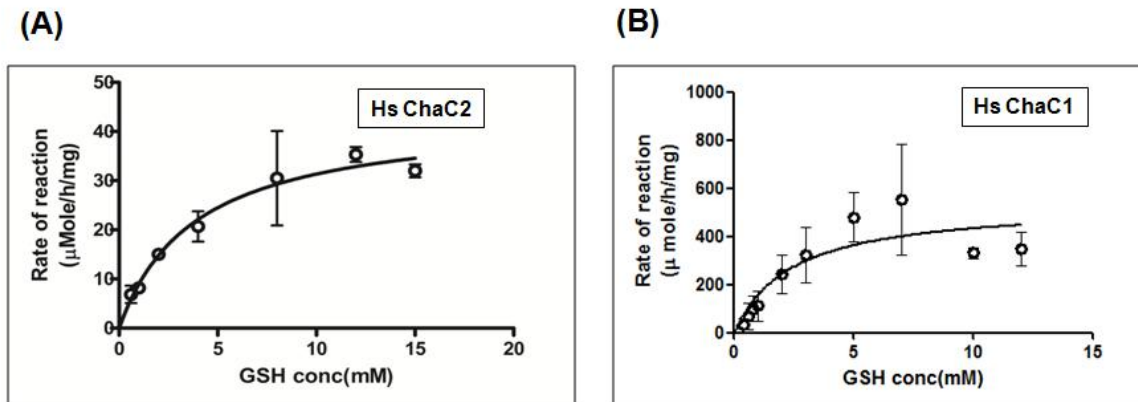


**FIGURE 1.** NJ based phylogenetic tree of ChaC1 and ChaC2 proteins. The NJ based tree was created using MEGA6 software with 1000 bootstrappings. Two distinct members of ChaC family are marked and bootstrap values are indicated respectively. The abbreviations used are Dm-*Drosophila melanogaster*, Hs-*Homo sapiens*, Mm-*Mus musculus*, Dr-*Danio rerio*, Rn-*Rattus norvegicus*, Ce-*Caenorhabditis elegans*, At-*Arabidopsis thaliana*, Dm-*Drosophila melanogaste*, Sc-*Saccharomyces cerevisiae*, Ca-*Candida albicans*, Ss-*Sus scrofa*, Ec- *Escherichia coli*, Bt-*Bos taurus*. Hs ChaC1,AAH19625.1; Hs ChaC1V1,NP\_077016.2; Hs ChaC2, NP\_001008708.1; Sc Gcg1, NP\_011090.3, Mm aChaC2i,NP\_080803.1; Mm bChaC2i,NP\_001277596.1; Dm ChaC2, NP\_651176.1; Ca ChaC2, NP\_503578.1; Bt ChaC1,NP\_001092352.1; Bt ChaC2,NP\_001068996.1; Ss ChaC1,XP\_005659810.1; Mm ChaC1,NP\_081205.1; RnChaC1, NP\_001020187.1; Dr ChaC1, NP\_001103596.2; BtChaC2, NP\_001068996.1; Ss ChaC2,XP\_003125197.1; Ec ChaC,NP\_415736.2; Rn ChaC1,NP\_001166908.1; Rn ChaC2,NP\_001020187.1; At 3GGCT2,NP\_564490.1; At 2GGCT2, NP\_567871.1; At1GGCT2,NP\_197994.1; Ce ChaC,NP\_503578.1; Dr ChaC2,NP\_001025128.1.

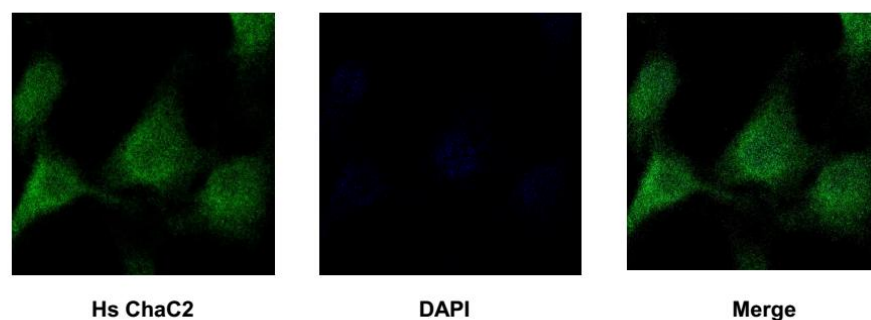
Figure 2



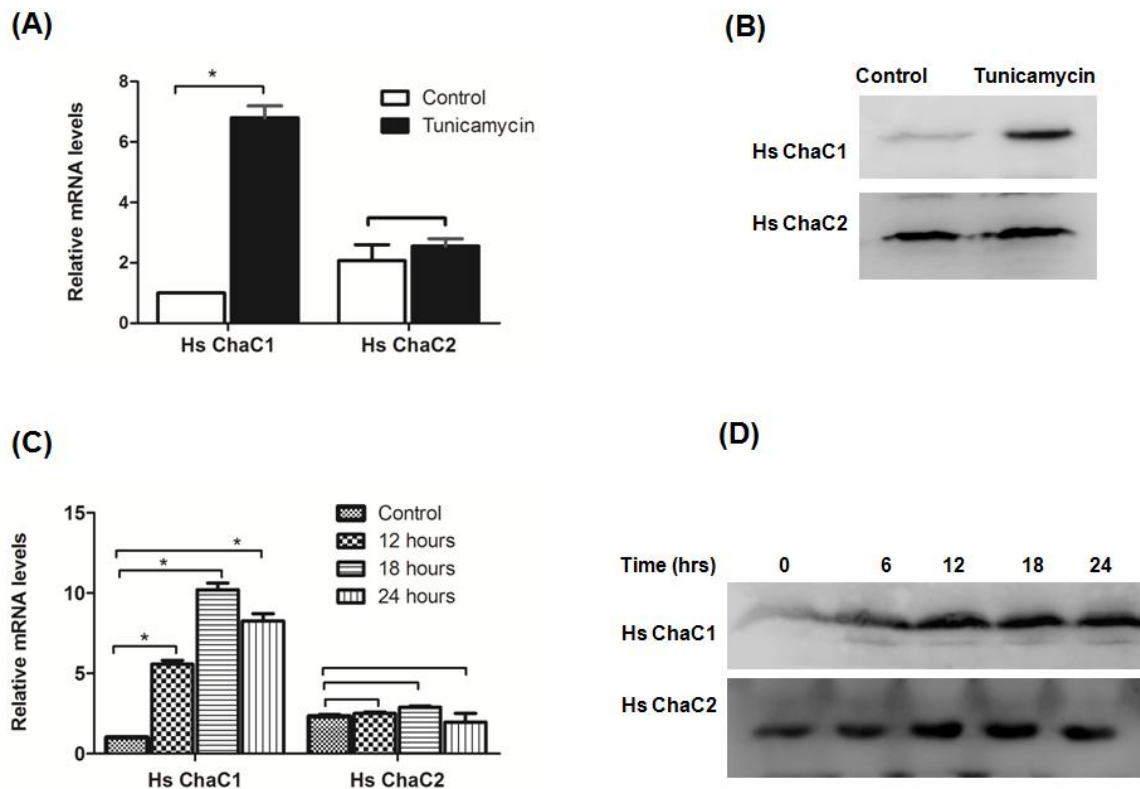
**FIGURE 2:** (A) *In vivo* growth assay in *S. cerevisiae* strain to check glutathione degradation function of human ChaC1 and ChaC2: *S. cerevisiae* strain ABC1723 was transformed with p416TEF harbouring human ChaC1 and ChaC2. The transformants were serially diluted and spotted on SD medium plate containing glutathione or methionine or  $\gamma$ -Glu-Met as a sulphur source. (B) *In vivo* growth assay in *S. cerevisiae* strain ABC1195 (*MATa his3 $\Delta$ 1 lys2 $\Delta$ 0 met15 $\Delta$ 0 ura3 $\Delta$ 0 gsh1  $\Delta$ ::LEU2*) to check glutathione degrading efficiencies. Transformants were grown in SD media containing GSH, serially diluted and spotted on SD plate containing 20 $\mu$ M GSH. (C) ROS levels in yeast cells (ABC1195) expressing human ChaC1 and ChaC2: ROS levels were measured using DCF-DA probe. (D) Glutathione levels of yeast BY 4741 transformed with Human ChaC1 and ChaC2. Lysates from the yeast transformants were used for glutathione estimation as explained in experimental procedures. The two datasets for each sample from two independent experiments were obtained and plotted using graph pad prism software (\* indicates P-value less than 0.05).

**Figure 3**

**FIGURE 3 :** Michaelis–Menten plot of (A) human ChaC2 and (B) human ChaC1 for glutathione: Human ChaC2 and human ChaC1 proteins were used for kinetic studies. Different concentrations of glutathione ranging from 0.6mM to 15mM were used. Dug1p coupled assay was used to estimate cysteine released as described in experimental procedures. Datasets of three independent experiments were analyzed using non linear regression (by Graphpad prism5).

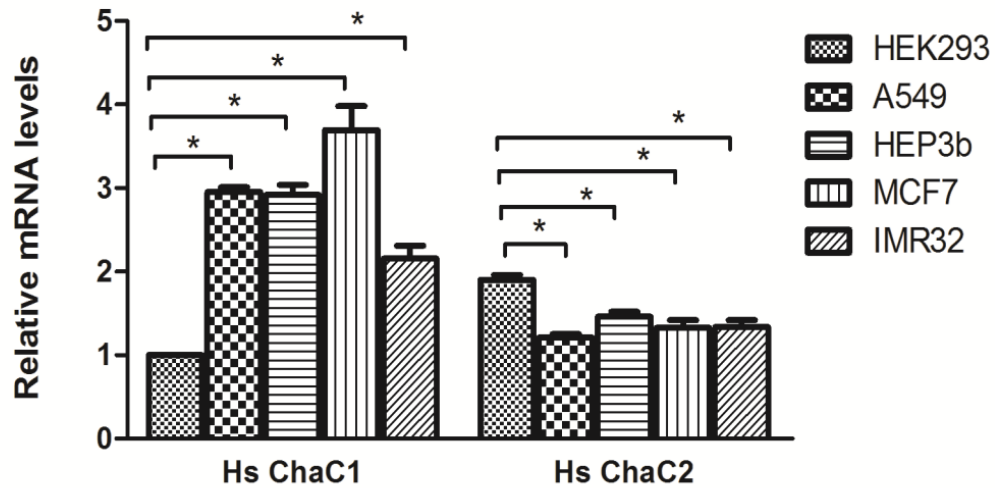
**Figure 4**

**FIGURE 4.** Cytosolic expression of human ChaC2. Expression of human ChaC2 in cytosol was confirmed by fluorescent microscopy. HEK cells immunostained with anti ChaC2 antibody displayed staining throughout cytoplasm. DAPI counterstaining was done to show the location of nucleus.

**Figure 5**

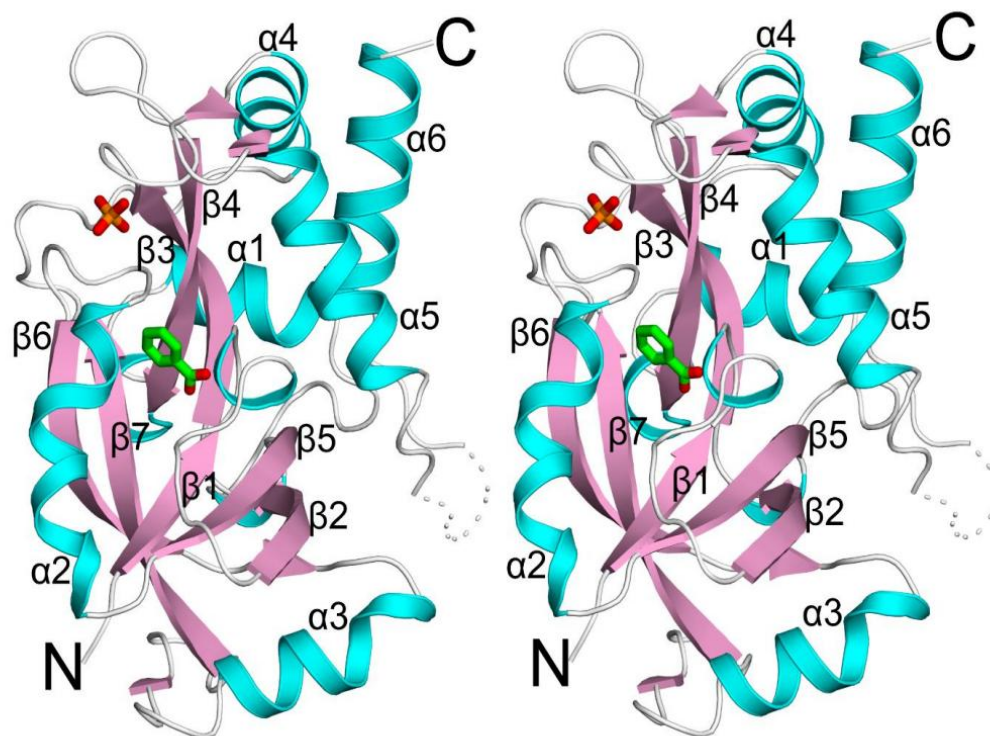
**FIGURE 5 :** Human ChaC1 but not human ChaC2 is induced specifically by ER stress inducers: Cells (HEK293) were cultured in untreated media (control) and in media containing Tunicamycin. (A) RNA and (B) protein levels were measured at different time intervals using real time PCR and western blot analysis respectively. (C,D) Regulation of human ChaC1 and ChaC2 under sulphur starvation conditions: Cells (HEK293) were cultured in media which lacks sulphur sources. (C) RNA and (D) protein levels were measured at different time intervals using real time PCR and western blot analysis. The data set obtained from three independent experiments were plotted using Graphpad prism5 software (\* indicates a P- value less than 0.05).

Figure 6



**FIGURE 6:** Comparison of human ChaC1 and ChaC2 expression in different cell lines: Expression levels were compared between HEK293, a non tumourigenic cell line and tumourigenic cell lines A549 (lung adenocarcinoma) Hep3b (Hepatocellular carcinoma) MCF7 (Breast adenocarcinoma) IMR32 (neuroblastoma) cell lines by measuring RNA levels using real time qPCR. The experiments were carried out in duplicates (\* indicates a P- value less than 0.05).

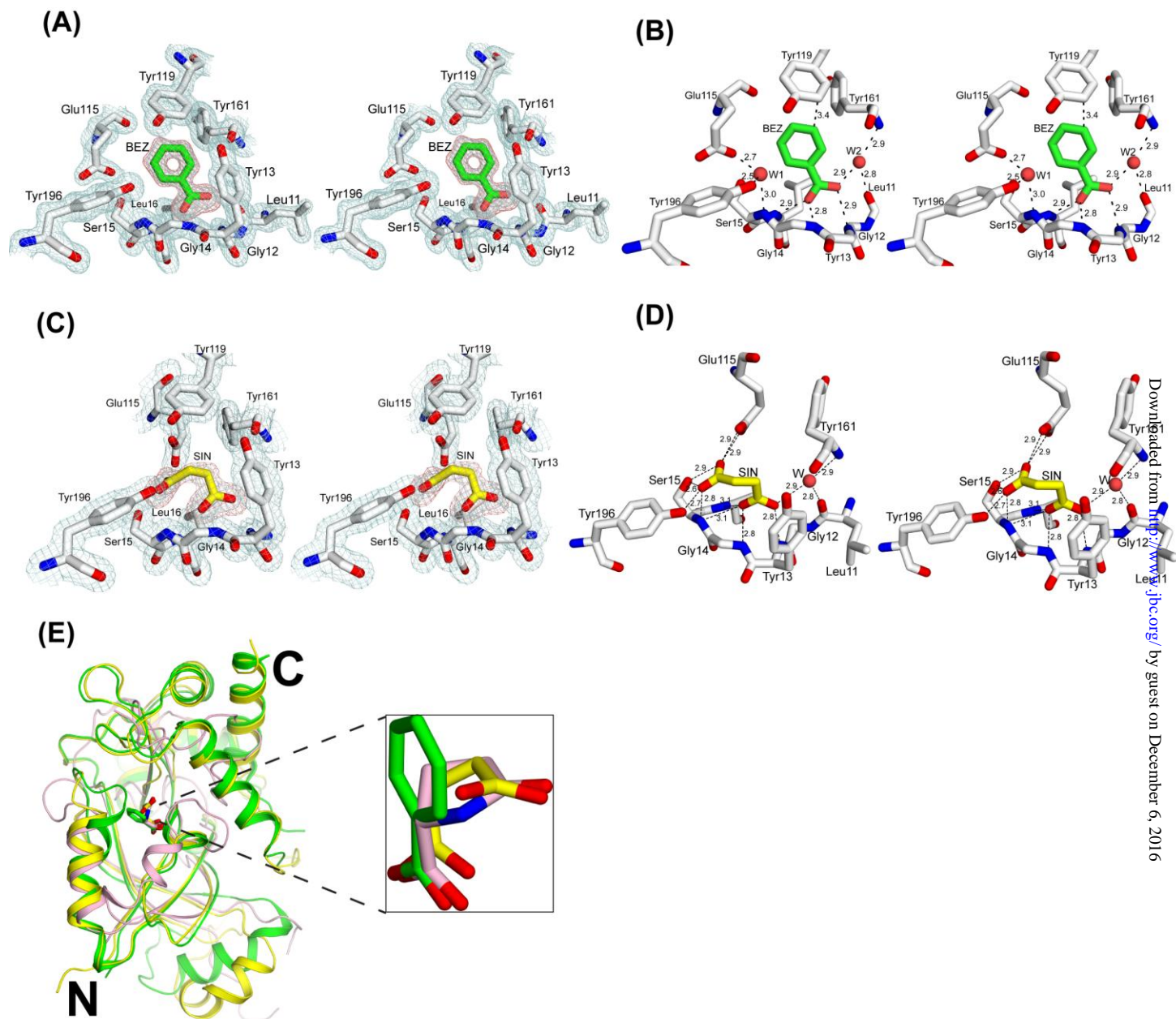
Figure 7



**FIGURE 7.** Crystal structure of GCG1. Stereo diagram showing the overall fold of GCG1 in cartoon form. The secondary structures are shown in cyan, pink and white for helices, strands and loops respectively. The benzoic acid (green) and phosphate ion (orange) are shown in stick model. The figure was generated using pyMOL (42)



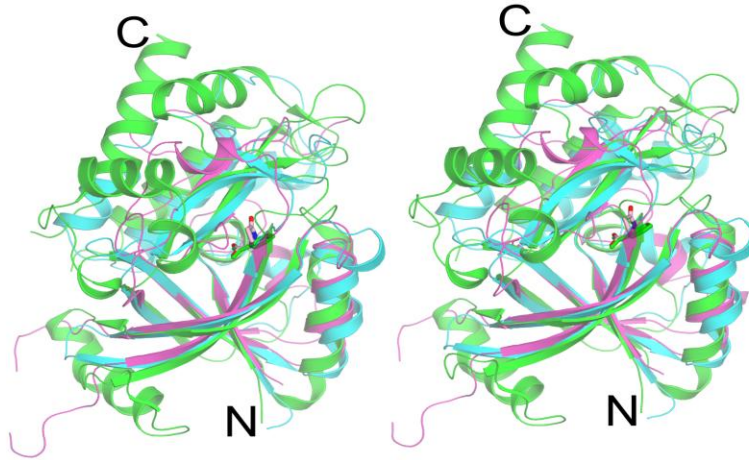
Figure 8



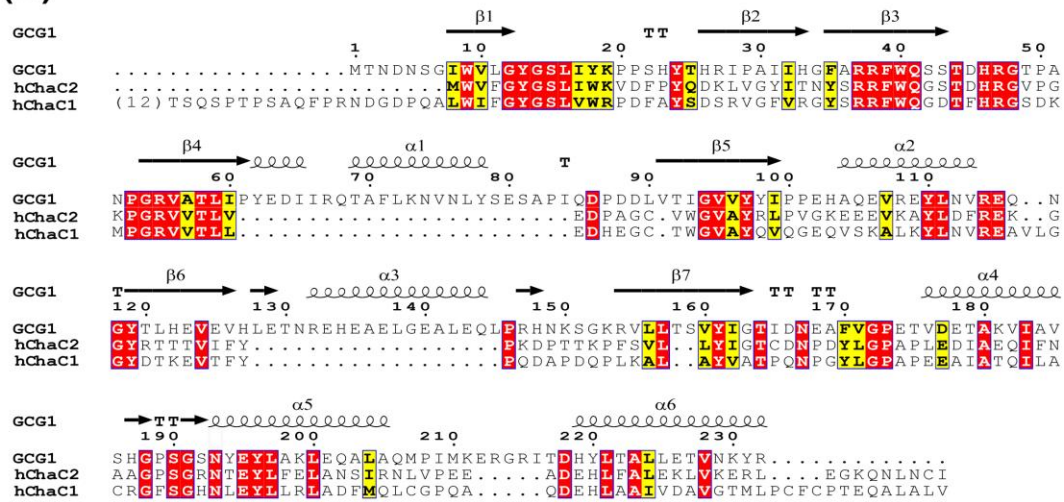
**FIGURE 8.** Catalytic site of GCG1. (A) Stereo diagram showing the omit map overlaid on the catalytic site of GCG1. The omit map was generated by deleting the benzoic acid (BEZ) from the model and refined with simulated annealing. The resultant Fourier (palecyan) and difference Fourier (salmon) maps contoured at 1.5 and 3.0  $\sigma$  level respectively are displayed around the catalytic site. The benzoic acid (BEZ) is shown in green. The electron density for water molecules are not shown for clarity purpose. (B) Stereo diagram showing the hydrogen bond interactions between benzoic acid (green) and residues from GCG1 (white). The side chain for some residues are not shown for clarity purpose. (C) Stereo diagram showing the omit map overlaid on the catalytic site of semet-GCG1-mutant. The omit map was generated by deleting the succinic acid (SIN) from the model and refined with simulated annealing. The resultant Fourier (palecyan) and difference Fourier (salmon) maps were displayed at 1.0 and 3.0  $\sigma$  level respectively. The succinic acid (SIN) is shown in yellow. (D) Stereo diagram showing the hydrogen bond interactions between succinic acid (yellow) and residues from semet-GCG1-mutant (white). (E) Superposition of benzoic acid that was bound with GCG1 (green), succinic acid that was bound with GCG1 (yellow) and 5-oxo-proline that was bound with GGACT (light pink). The inset shows the close view of superimposed ligands of benzoic acid (green), succinic acid (yellow) and 5-oxo-proline (light pink).

Figure 9

(A)



(B)



(C)

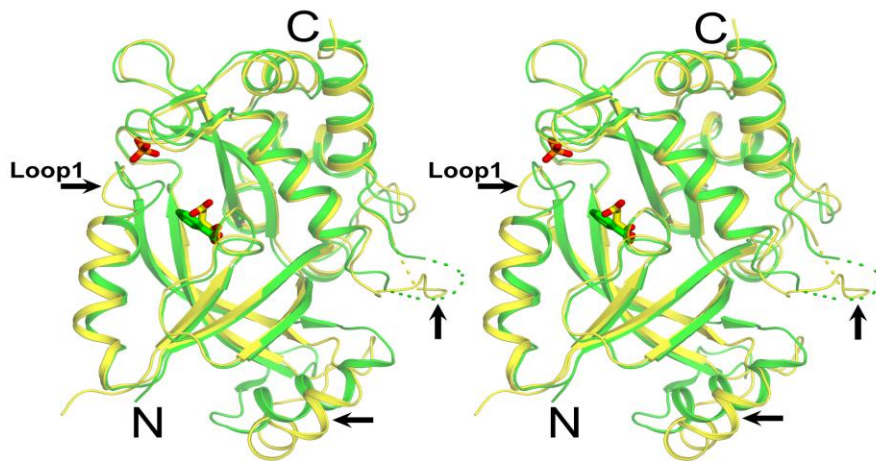


**FIGURE 9.** Comparison of members of  $\gamma$ -glutamylcyclotransferase. (A) Stereo diagram showing the superposition GCG1 (green),  $\gamma$ -glutamylcyclotransferase (cyan) and  $\gamma$ -glutamylamine cyclotransferase (light pink). The benzoic acid (green) bound at the catalytic site is shown in stick model. (B) Multiple sequence alignment of GCG1 and its homologues. Identical residues were shown in red background while similar residues were shown in yellow background. The secondary structure of GCG1 was marked on the top of the alignment. The residues were aligned using T-coffee software and merged with secondary structure using ESPript (43). (C) Stereo diagram in cartoon form showing the superposition of GCG1 (green) and semet-GCG1-mutant (yellow). The subtle conformational change of loop regions are marked with arrows. The benzoic acid (green) and succinic acid (yellow) bound at the catalytic site of GCG1 and semet-GCG1-mutant are shown in stick model.

## **ChaC2: An Enzyme for Slow Turnover of Cytosolic Glutathione**

Amandeep Kaur, Ruchi Gautam, Ritika Srivastava, Avinash Chandel, Akhilesh Kumar,  
Subramanian Karthikeyan and Anand Kumar Bachhawat

*J. Biol. Chem.* published online December 2, 2016

---

Access the most updated version of this article at doi: [10.1074/jbc.M116.727479](https://doi.org/10.1074/jbc.M116.727479)

### Alerts:

- [When this article is cited](#)
- [When a correction for this article is posted](#)

[Click here](#) to choose from all of JBC's e-mail alerts

This article cites 0 references, 0 of which can be accessed free at  
<http://www.jbc.org/content/early/2016/12/02/jbc.M116.727479.full.html#ref-list-1>